metabolites

MDPI

Review

Non-Invasive Analysis of Human Liver Metabolism by Magnetic Resonance Spectroscopy

John G. Jones

CNC—Center for Neuroscience and Cell Biology, CIBB—Centre for Innovative Biomedicine and Biotechnology, University of Coimbra, 3004-504 Coimbra, Portugal; john.griffith.jones@gmail.com; Tel.: +351-231-249-181

Abstract: The liver is a key node of whole-body nutrient and fuel metabolism and is also the principal site for detoxification of xenobiotic compounds. As such, hepatic metabolite concentrations and/or turnover rates inform on the status of both hepatic and systemic metabolic diseases as well as the disposition of medications. As a tool to better understand liver metabolism in these settings, in vivo magnetic resonance spectroscopy (MRS) offers a non-invasive means of monitoring hepatic metabolic activity in real time both by direct observation of concentrations and dynamics of specific metabolites as well as by observation of their enrichment by stable isotope tracers. This review summarizes the applications and advances in human liver metabolic studies by in vivo MRS over the past 35 years and discusses future directions and opportunities that will be opened by the development of ultra-high field MR systems and by hyperpolarized stable isotope tracers.

Keywords: in vivo magnetic resonance; liver metabolism; hyperpolarization; stable isotopes

Citation: Jones, J.G. Non-Invasive Analysis of Human Liver Metabolism by Magnetic Resonance Spectroscopy. *Metabolites* **2021**, *11*, 751. https://doi.org/10.3390/metabo11110751

Academic Editors: Jeanine J Prompers and Martin Kršňák

Received: 8 October 2021
Accepted: 26 October 2021
Published: 29 October 2021

1. Introduction

The liver represents a key metabolic node in the body encompassing nutrient transformation and fuel homeostasis as well as detoxification of ethanol and xenobiotic compounds. Its relatively large size and body location, coupled with a dynamic metabolome that features high concentrations of a diversity of metabolites such as glycogen, glutamine, ATP, sugar phosphates, phosphocholine and phosphoethanolamine, has made it an attractive target for in vivo magnetic resonance spectroscopy (MRS) studies of hepatic metabolism since the early days of in vivo MRS development [1–4]. Given that many diseases cause substantial changes in hepatic intermediary metabolism coupled with the availability of higher-field MRS systems for both in vivo human and animal model studies, there is high and ongoing interest in applying this methodology to further our understanding of hepatic intermediary metabolism in physiological and pathophysiological settings. The purpose of this review is to highlight the versatility of multinuclear in vivo MRS both in direct observation of hepatic metabolites as well as hepatic metabolite enrichment from metabolic stable-isotope tracers.

1.1. Observation of Hepatic Metabolites by MRS

There are several aspects that increase the difficulty of performing in vivo MRS spectroscopy of the liver compared to other large organs such as the brain. These have been previously discussed in detail [5] and can be summarized as follows: First, there is considerable inter-individual variability in its gross structure (i.e., configuration of the lobes and major vessels, therefore the region for observation must be carefully tailored for each individual with particular attention to exclude extra-hepatic tissues such as muscle or adipose tissue. Second, in a resting supine individual, the liver position is not static. This is primarily due to diaphragm movement during breathing but other involuntary processes such as intestinal peristalsis and pulsatile blood flow also contribute. This affects ^{1}H signals in particular hence ^{1}H MRS data are typically acquired periodically while the subject holds

their breath [5–8]. Thirdly, the liver has higher levels of iron compared to many other tissues which results in paramagnetic broadening of MR signals.

1.2. Advances in MRS Instrumentation

Since the development of whole-body MR scanners with fields of 0.5–1.5 T in the 1980's, there has been a constant push for systems with ever higher magnetic fields. Currently, 3 T systems are becoming widespread and in 2017, the Food and Drugs Administration approved a 7 T system as a magnetic resonance imaging device. As of now (2021), the highest operating field for human subjects is 10.5 T at the University of Minnesota facility, and initial studies indicate that subject safety is not compromised in this setting [9]. There are ongoing efforts to develop systems of 11.7 T (AROMA consortium H2020 grant agreement No 885876) and initiatives for the development of 14–20 T systems [10]. For in vivo MRS spectroscopy, higher magnetic fields deliver an increase in signal dispersion that scales directly with the increase in the applied field (B_0) while the signal-to-noise ratio (SNR) increases as $B_0^{1.65}$ [11]. At the same time, there is also the need for increased radiofrequency (RF) power deposition that may exceed safety limits. This is primarily an issue for broad-band decoupling of high-gamma nuclei such as ^{1}H. In addition, establishing field homogeneity and operating imaging gradients for localized spectroscopy is more challenging at higher fields. Among other things, this increases the difficulty of obtaining narrow MR signals from deeper hepatic regions. Finally, both spin-lattice (T_1) and transverse relaxation times (T_2) of many metabolites are sensitive to magnetic field strength [12,13] which can compromise the efficacy of signal collection and alter the relationship between signal intensity and metabolite concentration. To date, there is a strong consensus that the advantages of higher fields far outweigh these drawbacks, particularly for MRS with low-gamma nuclei [10,11,14].

Since high field MRS has been primarily driven by studies on the brain, the integral RF transmit/receive components of high field instruments are optimized for the head rather than the abdominal region. Therefore, liver MRS studies with these systems have required the development of bespoke RF coils and antenna systems [15–17].

1.3. In Vivo ^{1}H MRS of Liver

^{1}H is the default observation nucleus for clinical imaging and ^{1}H body coils are also a standard feature for clinical 1.5–3.0 T MR systems. Thus, it is usually feasible to acquire localized ^{1}H spectra of liver tissue on a standard hospital MR scanner.

1.3.1. ^{1}H MRS of Liver Lipids

To date, the most widespread application, and perhaps among the most important in terms of current clinical relevance, is the quantification of liver triglycerides. ^{1}H MRS provides a precise measurement of liver triglyceride levels, with better sensitivity and specificity than other noninvasive probes of liver fat such as ultrasound [18]. This approach was initially validated in a large population (2349 participants) and established the now widely accepted threshold of 55.56 mg/g liver triglycerides concentration for non-alcoholic fatty liver disease (NAFLD), based on triglycerides concentrations measured for the 95th percentile of this study cohort [19]. More recently, the detection of the triglyceride signal has been translated into an imaging modality (magnetic resonance imaging-proton density fat fraction, MRI-PDFF) that provides information on the whole liver combined with simpler post-acquisition processing and representation of the data [20]. MRI-PDFF is now considered as the gold standard for hepatic lipid quantification in various settings [21,22]. At fields of 3 T and above, signals from mono- and polyunsaturated fatty acids become resolved allowing the abundance of these species to be measured thereby providing a lipidomic profile in addition to total liver triglycerides levels [23,24].

1.3.2. ^{1}H MRS of Other Hepatic Metabolites

Aside from triglycerides, other hepatic metabolites that have been quantified by ^{1}H MRS include choline-containing compounds and glycogen [25–27] which were measured with a 3 T instrument. While many tumors have high levels of choline, in vivo ^{1}H MRS measurements of hepatic choline in patients with liver tumors did not observe any significant increases in choline compared to healthy subjects [27]. Glycogen observation by conventional in vivo ^{1}H MRS is hampered by several factors including short T_2 of its hydrogens and a significant loss of signal during presaturation of the water signal due to saturation transfer [28]. By applying this process in reverse, i.e., pre-saturating the glycogen signals and observing the resulting decrease in the water signal intensity, Zhou et al. were able to follow dynamic changes in hepatic glycogen levels induced by glucagon and fasting re-feeding [29]. Since this approach only requires the quantification of the water signal, it can also be easily translated into an imaging mode.

1.4. In Vivo ^{31}P MRS of Liver

^{31}P is the sole stable isotope of phosphorus with a nuclear spin of $\frac{1}{2}$ and a relatively strong gyromagnetic ratio (40.5% that of ^{1}H). Although the ^{31}P chemical shift dispersion is much greater than that of ^{1}H (~350 ppm versus ~10 ppm), metabolites of phosphorus all resonate within a 25 ppm spectral region, with phosphate mono- and diester species crowded into a ~5 ppm window. The chemical shift of inorganic phosphate (P_i) as well as those of phosphate esters are also sensitive to pH [30,31] while those of phosphoanhydrides are influenced by the binding of various metal ions such as magnesium [32]. Saturation transfer experiments allow the transfer of phosphorus from one metabolic intermediate to another to be followed thereby providing information on rates of synthesis such as that of ATP from ADP and P_i [33–36]. Therefore, in addition to assaying key phosphometabolites with good precision and accuracy [37], in vivo ^{31}P MRS also informs on bioenergetic status and ionic homeostasis. The ratio of phosphodiesters to phosphomonoesters signals (PDE/PME) is linked to cell membrane turnover [38,39]. PDE/PME of cirrhotic and of cancerous liver tissues were shown to differ significantly from that of a healthy liver [40–42]. While high resolution ^{31}P NMR of liver extracts can identify over 50 different phosphometabolites [43], the number of metabolites that can be resolved and quantified by in vivo ^{31}P MRS is far less [44] but is nevertheless more diverse in comparison to that provided by ^{1}H MRS. At high magnetic fields ($\geq$7 T), the increased signal dispersion allows more hepatic phospho-metabolites to be resolved and quantified, [45,46] as exemplified by Figure 1 [46].

The challenges and potential limiting factors of high-field in vivo ^{31}P NMR MRS include design and implementation of RF hardware for optimal observation of hepatic metabolites, avoidance of confounding signals from non-hepatic tissues in intimate contact with the liver such as phosphatidylcholine from the gall-bladder and phosphcreatine from surrounding muscle [4,47,48]; and maintaining efficient ^{1}H-decoupling without exceeding the safe limits for tissue RF power deposition. Finally, there are hepatic studies that integrate the observation of ^{31}P and ^{1}H thereby providing correlated information of phospho-metabolites with other species such as lipids [49–51]. A portfolio of in vivo ^{31}P MRS studies of human liver is shown in Table 1. This is not meant to include all reported studies to date, but instead to highlight the diversity of topics in hepatic physiology and intermediary metabolism that have been studied.

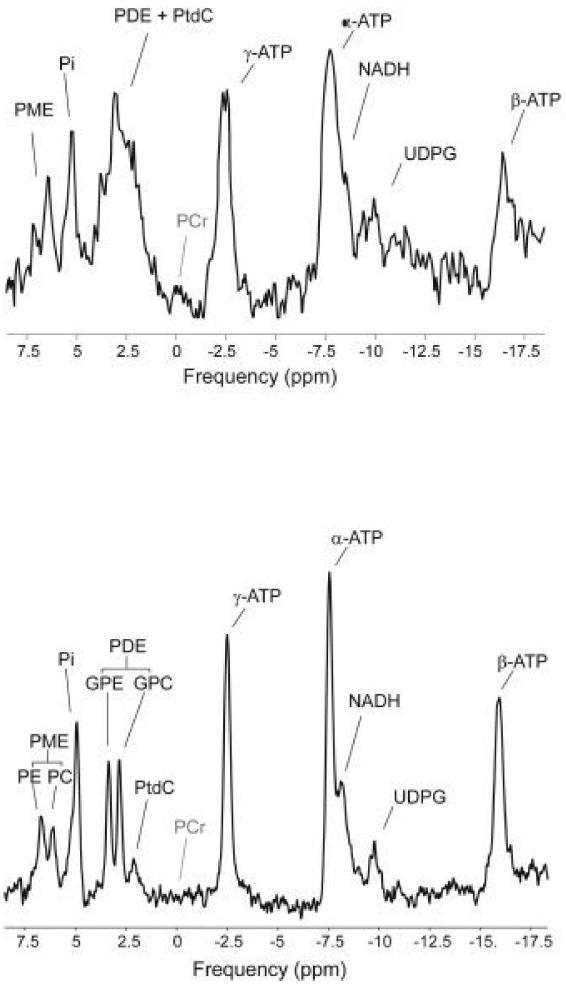

Figure 1. Comparison of in vivo ^{31}P MR spectra of human liver acquired at 3 T (**top**) and at 7 T (**bottom**). This figure was adapted from ref. [39].

Table 1. Selected in vivo ^{31}P MRS studies of liver metabolism in human subjects.

Study Description	Main Findings	Field Strength (T)	Reference
Effects of a lipid-rich breakfast meal followed by exercise on hepatic ATP and lipid levels for healthy subjects.	Liver fat increased postprandially and continued to increase during exercise. Liver ATP did not change from fasting to postprandial state, but significantly decreased after exercise.	3.0	[51]
Effect of a oral fructose challenge on hepatic ATP reserves in healthy subjects. Baseline liver glycogen was also measured by ^{13}C NMR	Hepatic ATP levels dropped by ~20% from baseline and reached a minimum value 50 min after the load. The time to reach minimum ATP levels was inversely correlated with subject BMI. ATP recovery rate was inversely correlated with baseline glycogen levels.	3.0	[52]
Effects of acute fructose ingestion with and without an accompanying load of ethanol on liver P-metabolite dynamics in healthy subjects.	Over a 40 min interval post load, P-metabolites were measured with 5 min time resolution. While ethanol had no effects on rates of phosphomonester (PME) formation and ATP depletion resulting from fructose metabolism, it significantly slowed down the rate of PME degradation.	1.5	[53]

Table 1. *Cont.*

Study Description	Main Findings	Field Strength (T)	Reference
Characterization of P-metabolites and ATP fluxes and correlation with lipid levels determined by ^{1}H MR and biopsy evaluation in subjects with NAFLD and NASH	Several PME and PDE ^{31}P signals were resolved and quantified as well as those from NADPH and UDPG. Significant differences in relative abundances of PME phosphoethanolamine (PE) and ATP between NAFLD and NASH. Significantly lower rates of ATP synthesis fluxes in NASH compared to NAFLD subjects [33]. In another ^{31}P MRS study performed at 3 T, levels of NADPH, a marker of inflammation and fibrosis, were elevated in NASH patients compared to healthy controls [54].	7.0, 3.0 (^{31}P) 3.0 (^{1}H)	[33,54]
Characterization of PME profile in fasted subjects with compensated and decompensated cirrhosis following infusion with a gluconeogenic substrate—L-alanine.	At baseline, PME levels of both compensated and decompensated cirrhotic subjects were elevated compared to healthy controls. After L-alanine infusion, PME levels of healthy controls were significantly increased, consistent with gluconeogenic activity. This increase was significantly smaller for patients with compensated cirrhosis and was absent in patients with decompensated cirrhosis.	1.5	[55]
Characterization of P-metabolites in pediatric liver transplant patients with different outcomes of graft function	Patients with impaired graft function had elevated PME/total phosphate compared to those with good graft function and to healthy controls.	1.5	[56]
Effects of intravenous ATP infusion for 22–24 h on liver energy status in advanced lung cancer patients.	Liver ATP levels were significantly increased following ATP infusion to levels that were similar to those of healthy subjects. This effect was greatest for patients that were undergoing weight loss and who had the lowest baseline ATP liver levels	1.5	[57]

1.5. In Vivo ^{13}C MRS of Liver

^{13}C is the stable isotope of carbon with a spin of $\frac{1}{2}$ and a natural abundance of 1.1%. Its gyromagnetic ratio is ~$\frac{1}{4}$ that of ^{1}H, therefore its overall sensitivity is several orders of magnitude less than that of ^{1}H. Nevertheless, for liver metabolites that can reach high concentrations, such as glycogen and lipids, their natural abundance ^{13}C signals can be observed with reasonable collection times [2,3,58]. In addition, ^{13}C signals from isotopically enriched substrates and their metabolic products, where ^{13}C abundance can be boosted to nearly 100-fold over background levels, can be detected [59–63].

The ^{13}C chemical shift dispersion is much greater in comparison to ^{1}H, therefore in principle it provides increased resolution of metabolites. On the other hand, the majority of metabolite carbons are bound to one or more hydrogens that result in the ^{13}C signal being split by ^{1}H-^{13}C scalar coupling. Not only does this effectively reduce the signal-to-noise ratio by at least a factor of two, it also multiplies the number of metabolite signals within the same spectral region thereby compromising signal resolution. These effects can be eliminated by broadband ^{1}H-decoupling which also provides an additional boost to the ^{1}H-decopuled ^{13}C singlet signal by the nuclear Overhauser enhancement (nOe) effect. As magnetic fields increase, the ^{1}H-frequency decoupling bandwidth also needs to be increased resulting in higher deposition of RF power into tissues. Moreover, nOe can vary substantially between ^{13}C in different molecular sites, and this must be taken into account when relating ^{13}C signal intensities to absolute metabolite concentrations. Finally, the T_1 of non-protonated carbons such as carboxyls and quaternary carbons are relatively

long, which in combination with an absence of nOe, can constrain the acquisition of their ^{13}C signals over short intervals. In vivo ^{13}C MR of hepatic metabolism in humans is being driven forward by several innovations that directly confront the limitations described earlier. To minimize the deposition of RF power into the region of observation as a result of broadband ^{1}H decoupling, bespoke decoupling schemes have been developed [64]. For studies that focus on observation of a single metabolite ^{13}C signal, such as the carbon 1 resonance of glycogen, it is only necessary to decouple the hydrogen attached to this carbon, hence the decoupling bandwidth—and, therefore the power deposition—can be substantially reduced. This approach was used in one of the pioneering in vivo ^{13}C MR studies of liver metabolism, which documented the decrease in the natural-abundance ^{13}C1 signal of liver glycogen during fasting in healthy humans [3]. Hepatic glycogen synthesis and degradation fluxes are key components of systemic glucose homeostasis and are highly sensitive to the insulin/glucagon ratio. The application of in vivo ^{13}C MR to measure changes in hepatic glycogen during fasting and feeding has advanced our understanding of hepatic carbohydrate metabolism in subjects with insulin resistance, as well as in patients with diabetes [65–69]. Among other things, it revealed that while both hepatic glycogen deposition and degradation rates are significantly reduced in Type-1 diabetic subjects undergoing standard insulin therapy, these fluxes may be restored to normal with intensive insulin therapy [70,71]. Acute induction of hepatic insulin resistance via infusion of lipid was shown to modify rates of hepatic glycogenolysis in the fasted state [68,72].

In some cases, ^{13}C-signals of ^{13}C-enriched hepatic metabolites can be resolved and quantified in the absence of ^{1}H-decoupling. For example, the appearance of ingested [1-^{13}C]glucose in the liver and its conversion to [1-^{13}C]glycogen was observed at 3 T with 0.5 min time resolution without deployment of ^{1}H decoupling [59]. In a study of hepatic Krebs cycle metabolism with [1-^{13}C]acetate, ^{13}C appearance in the two carboxyls of glutamate was monitored [62]. Since ^{13}C nuclei in these sites have no directly attached protons, optimal observation of their ^{13}C signals is not dependent on ^{1}H decoupling.

The interaction of ^{13}C and ^{1}H via scalar coupling provides the basis for monitoring ^{13}C-enrichment indirectly via observation of the attached proton(s). While ^{1}H observation delivers vastly increased signal sensitivity and is also the default nucleus for in vivo localized spectroscopy with whole-body MR systems, the pulse sequences for selecting the ^{1}H-^{13}C-coupled signals while filtering out those from ^{1}H-^{12}C are more complex and require precise calibration of the RF electronics. Although, in principle, the ^{1}H-^{13}C-coupled signals can be resolved along both ^{1}H and ^{13}C dimensions, for in vivo studies, time and instrument constraints limit the signal acquisition to the ^{1}H dimension only. Thus, the signal dispersion is limited to that of ^{1}H, which effectively precludes shotgun observation of arrays of ^{13}C-enriched metabolites but may, nevertheless be effective for observation of near-isochronous ^{13}C-enriched signals such as the methylene carbons of triglyceride fatty acids [73]. Veeraiah et al. applied a similar approach to demonstrate that the background ^{13}C-methylene signals of hepatic fatty acids in healthy subjects could be quantified in vivo with high sensitivity and minimal interference from ^{1}H-^{12}C signals [74].

The advent of hyperpolarization (HP), which can boost the difference in nuclear spin populations between the two spin states of the ^{13}C nucleus by several orders of magnitude over that achieved by an applied magnetic field, provides correspondingly huge gains in sensitivity for observation of ^{13}C-enriched substrates. However, this advantage can only be realized over a relatively limited time window that is ultimately constrained by the longitudinal relaxation time (T_1) of the observed ^{13}C species. Since ^{13}C-^{1}H dipolar interactions promote the relaxation of the ^{13}C, thereby shortening T_1, HP studies utilize ^{13}C-enriched substrates containing ^{13}C that are not directly bound to protons. These nuclei are relaxed via the less efficient chemical shift anisotropy mechanism, resulting in T_1 values that are several-fold longer compared to proton-bound ^{13}C nuclei, but nevertheless rarely exceeding 60 s—and moreover subject to significant reduction by high magnetic fields [75]. Since 99% of nuclear magnetization is lost over an interval of 5 $\times$ T_1, the challenges in rapid administration and in vivo observation of hyperpolarized ^{13}C-enriched substrates

are reminiscent of those encountered in positron emission tomography (PET) studies of short-lived nuclei such as ^{13}N and ^{11}C. To date, HP studies of liver metabolism with ^{13}C-enriched substrates have been limited to preclinical animal models. While dynamic nuclear polarization (DNP) is the principal method for generating hyperpolarized states in ^{13}C-enriched substrates, for certain substrates that can be synthesized via hydrogenation of a ^{13}C-enriched precursor, for example [1-^{13}C]fumarate from [1-^{13}C]acetylene dicarboxylate, polarization via the reductive addition of *para*-hydrogen is both faster and requires less costly equipment compared to DNP [76]. The principal obstacles in the translation of HP to humans have been in ensuring the safety and enabling of rapid delivery of hyperpolarized ^{13}C-enriched substrates. Both [1-^{13}C]- and [2-^{13}C]pyruvate have obtained regulatory approval by the FDA as substrates for hyperpolarized MRI [77]. In a study of patients with prostate cancer, delivery of hyperpolarized [1-^{13}C]pyruvate was not associated with any adverse events [78]. Given the diversity of pre-clinical studies of HP ^{13}C-enriched substrates in both perfused liver as well as in vivo, it is quite certain that this methodology will be applied to the study of human liver metabolism in the very near future.

1.6. In Vivo MRS of Other Nuclei in the Study of Hepatic Metabolism

1.6.1. Deuterium

Deuterium (^{2}H) is a quadrupolar nucleus with a spin of 1 and a gyromagnetic ratio that is ~15% that of ^{1}H. Its natural abundance is 0.015%, which alongside its limited dispersion (15% that of ^{1}H in terms of absolute frequency, Hz) makes it a poor choice for observation of liver metabolites compared to ^{31}P or natural abundance ^{13}C MRS. However, its low natural abundance also means that ^{2}H-enriched substrates, which are up to ~2000 times higher than the background, can be more effectively observed. In addition, ^{2}H T_1 values are much shorter compared to those of ^{1}H, ^{13}C, or ^{31}P allowing more free-induction decays to be collected per unit of time thereby effectively boosting sensitivity. However, for large molecular weight metabolites such as glycogen that exhibit very short spin-spin (T_2) relaxation times, MR visibility of the ^{2}H label may be severely compromised [79]. Since the coupling constants of ^{2}H with neighboring ^{1}H nuclei are relatively small, ^{2}H signals are not substantially degraded by these interactions and can therefore be observed in the absence of broadband ^{1}H decoupling. In terms of MR hardware, magnetic field strength is the most important limiting factor in the development of metabolic studies with ^{2}H-enriched tracers. De Feyter et al. obtained in vivo ^{2}H MR signals at a field of 4 T from human liver following ingestion of a glucose load enriched with [6,6-$^{2}H_2$]glucose [80]. Under these conditions, there was no resolution of [6,6-$^{2}H_2$]glucose and [6,6-$^{2}H_2$]glycogen signals, but given that [6,6-$^{2}H_2$]glycogen was likely not visible under the parameters used for observation, the signals were presumably those of [6,6-$^{2}H_2$]glucose.

In cases where the ^{2}H label can undergo exchange with ^{1}H, for example during conversion of [6,6-$^{2}H_2$]glucose to [3,3-$^{2}H_2$]lactate, where the [3,3-$^{2}H_2$]pyruvate intermediate can exchange its ^{2}H with ^{1}H body water, the product signal intensity needs to be corrected for this exchange [81]. Also, for ^{2}H-enriched substrates whose metabolism involves the cleavage of a ^{2}H-^{13}C-bond, for example conversion of [2-^{2}H]glucose-6-P to fructose-6-P via glucose-6-P isomerase [82] the presence of a significant kinetic isotope effect may substantially alter the rate of tracer metabolism relative to that being traced [81].

The study of liver metabolism can also be undertaken with deuterated water ($^{2}H_2O$). $^{2}H_2O$ is inexpensive and can be safely administered to 0.5% body water in humans (~33 times above background) over an indefinite period. The ubiquity of water and metabolite hydrogen exchanges in intermediary metabolic pathways results in the ^{2}H-enrichment of a diversity of metabolites including lipids and amino acids. Among other things, the rate of ^{2}H enrichment of a given metabolite informs its rate of synthesis and/or turnover. With the advent of very high fields (>10 T), it is likely that hepatic ^{2}H signals of metabolites enriched by $^{2}H_2O$ will be at least partially resolved in vivo for human subjects.

1.6.2. Fluorine

As for ^{31}P, fluorine exists in nature as single stable isotope, ^{19}F. It has a spin of $\frac{1}{2}$, and its sensitivity is 83% that of ^{1}H. It generates sharp NMR signals that cover a wide chemical shift range. Its relaxation properties are similar to that of ^{1}H, hence, conventional ^{1}H pulse sequences for quantitative measurement of ^{1}H metabolite signals can be easily adapted for ^{19}F. An adult human has ~2.6 g of fluorine that it is almost entirely distributed as fluoride in teeth and bone. Thus, soft biological tissues have essentially no background ^{19}F signal, therefore suppression of superfluous signals is not required and spectrometer sensitivity can be fully exploited.

Essentially all in vivo human studies involving ^{19}F have focused on the appearance and/or metabolism of pharmacological agents containing ^{19}F as part of their molecular composition. The first report describing the observation of hepatic ^{19}F signals in vivo was published by Wolf et al. in 1987 [83]. Three cancer patients were studied with a 1.5 T system following ingestion of the anti-cancer drug 5-fluoro uracil (5-FU). Subsequently, the kinetics of 5-FU appearance in the liver and its bio-transformation to 5-fluoro ureido propionic acid and α-fluoro-β-alanine were documented [84–88]. It was demonstrated that 5-FU was retained longer by tumor tissue compared to the surrounding healthy tissues [84] and that tumor 5-FU levels were positively correlated with the clinical response to treatment [87,89]. In vivo ^{19}F MR studies demonstrated that the lifetime of 5-FU within hepatic tumors could be extended by interferon-α [90] and by inhibitors of 5-FU catabolism [91]. In a study performed at 3 T, where different regions of the liver were assayed following ingestion of Capecitabine, a pro-drug that is metabolized to 5-FU via 5′-deoxyfluorocytidine 5′-deoxyfluorouridine, these intermediates, as well as products of 5-FU degradation such α-fluoro-β-alanine and 5-fluoro ureido propionic acid, were detected and quantified. These metabolites were found to be heterogeneously distributed in the liver [92].

Sitafloxacin is a broad-spectrum antibacterial agent that contains a fluorine atom in its chemical structure. Its appearance and washout in the liver was characterized in a group of healthy subjects with a 1.5 T system [93]. These parameters were found to be similar to that measured in plasma using HPLC indicating that this drug was not retained in the liver for any significant time [93]. Niflumic acid is a medication for alleviating pain in muscle and joints and has a trifluoromethyl functional group as part of its structure. A study of healthy male volunteers who ingested a single dose of Niflumic acid was performed at 1.59 T [94]. In addition to the appearance of a ^{19}F signal corresponding to niflumic acid, a second signal was observed and was identified as 4′-hydroxy niflumic acid (4-HNA). The washout kinetics of the secondary metabolite was much slower in comparison to that of niflumic acid, and was attributed to the fact that while the parent drug is rapidly cleared via blood and urine, 4-HNA is cleared via the biliary system. To the extent that 4-HNA is recirculated via enterohepatic biliary circulation, its net clearance from the region of observation is slowed down. The authors also acknowledged that the 4-HNA signal might at least in part be originating from the biliary system itself rather than from liver tissue.

2. Future Perspectives and Main Conclusions

The two key drivers for the advancement of in vivo MR studies of human liver metabolism are the development of ultra high field clinical MR systems (≥7.0 T) and the availability of hyperpolarized stable-isotope tracers. While each of these technical developments by themselves will undoubtedly advance the state-of-the-art, there is a high degree of synergy when both are combined. This is well illustrated by preclinical studies that have integrated hyperpolarized tracers with in vivo MR observation at mid- to high fields. While high field magnets and hyperpolarization systems come with substantially higher capital and operating costs compared to current clinical MR scanners, they could potentially compete with positron emission tomography (PET) for metabolic imaging applications.

One of the key roles of the liver is the regulation of endogenous glucose production and the control of gluconeogenic flux is a key component of this process. Current methodologies rely on measuring the appearance of a gluconeogenic tracer in plasma

glucose. For various technical and theoretical reasons, this measurement is limited to quasi steady-state conditions, such as after overnight fasting or during a glucose clamp. Thus, the transition from fasting to feeding, where hepatic carbohydrate metabolic fluxes must undergo acute rearrangements in order to maintain whole body glucose homeostasis—and is, therefore, the most critical and testing phase for glucoregulation—is little understood. The ability to observe fast real-time alterations in hepatic sugar phosphates and other metabolites following administration of tracers, such as [2-^{13}C]dihydroxyacetone [95–97], [1-^{13}C]pyruvate [98–100], and [1-^{13}C]gluconolactone [101], promises to be invaluable for unveiling the redirection of hepatic carbohydrate fluxes during the fasted to fed transition. Moreover, the direct observation of hepatic metabolites overcomes another important limitation of gluconeogenic tracer enrichment of blood glucose: the inability to resolve gluconeogenic activity of the liver from that of other tissues such as the kidney and intestine.

For chronic metabolic diseases such as non-alcoholic fatty liver disease (NAFLD) and Type 2 diabetes, there is now renewed focus on the function of hepatocyte mitochondria in these settings. The leakage of electrons from complexes I and III of the electron transport chain results in the generation of reactive oxygen species (ROS). In addition to damaging critical cellular infrastructure such as membrane lipids and DNA, ROS also promote inflammation and can trigger cellular apoptosis and autophagy. Thus, the development of noninvasive hepatic ROS probes, such as hyperpolarized thiourea [102], and markers of hepatic redox state, such as [1-^{13}C]alanine and [1-^{13}C]lactate [103], will provide a deeper insight on the role and status of hepatic ROS in various physiological and pathophysiological settings. The oxidation of long-chain fatty acids (LCFA) by hepatocyte mitochondria is a critical component in hepatic lipid homeostasis and ketone body generation, and is highly controlled by LCFA uptake via the carnitine shuttle. Defects in hepatic mitochondrial fatty acid oxidation are associated with increased levels of acylcarnitine intermediates [104–106]. Therefore, the development of probes for assessing hepatic carnitine metabolism, such as hyperpolarized ^{15}N-carnitine [107], can potentially provide information on the status of hepatic LCFA oxidation. Finally, oxidative and anaplerotic pyruvate metabolism—mediated by mitochondrial pyruvate dehydrogenase and pyruvate carboxylase, respectively—is a key node in the hepatic metabolic network. Among other things, it commits pyruvate to either a gluconeogenic or lipogenic fate. The metabolic path of hyperpolarized [1-^{13}C]pyruvate can be followed in real time [98], thus providing the potential for a deeper understanding on the role of this critical metabolic control point in various nutritional and disease settings [99,100,108].

After lung cancer, hepatocellular cancer (HCC) is the leading cause of cancer deaths in the world [109] with NAFLD being the most rapidly growing contributor to HCC mortality and morbidity [110]. Noninvasive in situ metabolic profiling of liver tumors will deepen our understanding of tumor physiology and response to therapy and preclincal proof-of-concept studies of hepatic tumors with hyperpolarized substrates are poised to be translated into the clincal setting. The selective uptake and retention of hyperpolarized ethyl [1,3-$^{13}C_2$]acetoacetate by tumor tissue over healthy hepatocytes [111] provides the basis for tumor metabolic contrast agent imaging and also reveals important differences in carboxyl esterase activities between tumors and healthy tissue that may be exploited for pharmacological targeting. Imaging of tissue pH from hyperpolarized $^{13}CO_2$ and bicarbonate delivered in the form of hyperpolarized ethyl acetyl carbonate [112] can potentially delineate tumor necrotic regions which are typically hypoxic and acidic and also increase resistance to therapy. Finally, the local recurrence of HCC following therapy is a frequent and ominous event. Thus, improving our understanding of how tumor cells resist therapy and detection of surviving latent tumor cells is of critical importance in achieving better outcomes. By identifying a characteristic metabolic profile for latent tumor cells via hyperpolarized [1-^{13}C]pyruvate that provides the basis for their metabolic imaging, Perkons et al. also demonstrated that metabolic reprogramming is a key component of tumor cell survival [113].

Main Conclusions

The non-invasive study of human liver metabolism by MRS has been an enduring effort since the initial development of clinical MR scanners. Ongoing technological advances in the design of MR components, such as magnets, RF coils, and gradient systems, are resulting in continuous improvements in the quality and reproducibility of liver metabolite measurements and are also allowing hitherto hidden aspects of liver metabolism to be glimpsed. For some of the most important and prevalent diseases of the current age—notably NAFLD and HCC—it is becoming increasingly clear that their progression is characterized by alterations in hepatic intermediary metabolic fluxes. Importantly, alterations in metabolic flux may not necessarily be accompanied by significant changes in metabolite concentrations. Improvements in sensitivity and resolution of hepatic metabolite enrichments from stable isotope tracers will drive the transition from quantifying metabolite pools, per se, to measuring carbon fluxes through these pools, thereby gaining a much deeper understanding of metabolic alterations in hepatic diseases.

Funding: This work was financed by the European Regional Development Fund (ERDF), through the Centro 2020 Regional Operational Programme through the COMPETE 2020—Operational Programme for Competitiveness and Internationalization and Portuguese national funds via FCT—Fundação para a Ciência e a Tecnologia, under projects POCI-01-0145-FEDER-028147, UIDB/04539/2020 and UIDP/04539/2020.

Conflicts of Interest: The author declares no conflict of interest.

References

1. Francis, I.R.; Chenevert, T.L.; Gubin, B.; Collomb, L.; Ensminger, W.; Walker-Andrews, S.; Glazer, G.M. Malignant hepatic tumors: P-31 MR spectroscopy with one-dimensional chemical shift imaging. *Radiology* **1991**, *180*, 341–344. [CrossRef] [PubMed]
2. Jue, T.; Rothman, D.L.; Tavitian, B.A.; Shulman, R.G. Natural-abundance 13C NMR study of glycogen repletion in human liver and muscle. *Proc. Natl. Acad. Sci. USA* **1989**, *86*, 1439–1442. [CrossRef]
3. Rothman, D.L.; Magnusson, I.; Katz, L.D.; Shulman, R.G.; Shulman, G.I. Quantitation of Hepatic Glycogenolysis and Gluconeogenesis in Fasting Humans with ^{13}C NMR. *Science* **1991**, *254*, 573–576. [CrossRef] [PubMed]
4. Jue, T.; Rothman, D.L.; Lohman, J.A.; Hughes, E.W.; Hanstock, C.C.; Shulman, R.G. Surface coil localization of ^{31}P NMR signals from orthotopic human kidney and liver. *Proc. Natl. Acad. Sci. USA* **1988**, *85*, 971–974. [CrossRef]
5. Fischbach, F.; Bruhn, H. Assessment of in vivo 1H magnetic resonance spectroscopy in the liver: A review. *Liver Int.* **2008**, *28*, 297–307. [CrossRef] [PubMed]
6. Xu, L.; Liu, B.; Huang, Y.; Liu, X.; Zhang, S.-W.; Xin, X.-G.; Zheng, J.-Z. 3.0 T proton magnetic resonance spectroscopy of the liver: Quantification of choline. *World J. Gastroenterol.* **2013**, *19*, 1472–1477. [CrossRef] [PubMed]
7. Fischbach, F.; Schirmer, T.; Thormann, M.; Freund, T.; Ricke, J.; Bruhn, H. Quantitative proton magnetic resonance spectroscopy of the normal liver and malignant hepatic lesions at 3.0 Tesla. *Eur. Radiol.* **2008**, *18*, 2549–2558. [CrossRef]
8. Munakata, T.; Griffiths, R.D.; Martin, P.A.; Jenkins, S.A.; Shields, R.; Edwards, R.H.T. Anin vivo ^{31}P MRS study of patients with liver cirrhosis: Progress towards a non-invasive assessment of disease severity. *NMR Biomed.* **1993**, *6*, 168–172. [CrossRef]
9. Grant, A.; Metzger, G.J.; Van de Moortele, P.-F.; Adriany, G.; Olman, C.; Zhang, L.; Koopermeiners, J.; Eryaman, Y.; Koeritzer, M.; Adams, M.E.; et al. 10.5 T MRI static field effects on human cognitive, vestibular, and physiological function. *Magn. Reson. Imaging* **2020**, *73*, 163–176. [CrossRef]
10. Budinger, T.F.; Bird, M.D.; Frydman, L.; Long, J.; Mareci, T.; Rooney, W.D.; Rosen, B.; Schenck, J.F.; Schepkin, V.D.; Sherry, D.; et al. Toward 20 T magnetic resonance for human brain studies: Opportunities for discovery and neuroscience rationale. *Magma Magn. Reson. Mater. Phys. Biol. Med.* **2016**, *29*, 617–639. [CrossRef]
11. Ladd, M.E.; Bachert, P.; Meyerspeer, M.; Moser, E.; Nagel, A.M.; Norris, D.G.; Schmitter, S.; Speck, O.; Straub, S.; Zaiss, M. Pros and cons of ultra-high-field MRI/MRS for human application. *Prog. Nucl. Magn. Reson. Spectrosc.* **2018**, *109*, 1–50. [CrossRef]
12. Lopez-Kolkovsky, A.L.; Mériaux, S.; Boumezbeur, F. Metabolite and macromolecule T1 and T2 relaxation times in the rat brain in vivo at 17.2T. *Magn. Reson. Med.* **2016**, *75*, 503–514. [CrossRef]
13. Pollack, M.H.; Jensen, J.E.; Simon, N.M.; Kaufman, R.E.; Renshaw, P.F. High-field MRS study of GABA, glutamate and glutamine in social anxiety disorder: Response to treatment with levetiracetam. *Prog. Neuro-Psychopharmacol. Biol. Psychiatry* **2008**, *32*, 739–743. [CrossRef]
14. Deelchand, D.K.; Uğurbil, K.; Henry, P.-G. Investigating brain metabolism at high fields using localized 13C NMR spectroscopy without H-1 decoupling. *Magn. Reson. Med.* **2006**, *55*, 279–286. [CrossRef] [PubMed]
15. Rivera, D.; Kalleveen, I.; de Castro, C.A.; van Laarhoven, H.; Klom, D.; van Der Kemp, W.; Stoker, J.; Nederveen, A. Inherently decoupled H-1 antennas and P-31 loops for metabolic imaging of liver metastasis at 7 T. *NMR Biomed.* **2020**, *33*, e4221. [CrossRef]

16. Van Houtum, Q.; Welting, D.; Gosselink, W.; Klomp, D.; De Castro, C.A.; Van Der Kemp, W. Low SAR ^{31}P (multi-echo) spectroscopic imaging using an integrated whole-body transmit coil at 7T. *NMR Biomed.* **2019**, *32*, e4178. [CrossRef] [PubMed]
17. Van Gorp, J.S.; Seevinck, P.R.; Andreychenko, A.; Raaijmakers, A.J.E.; Luijten, P.R.; Viergever, M.A.; Koopman, M.; Boer, V.O.; Klomp, D.W.J. ^{19}F MRSI of capecitabine in the liver at ^{7}T using broadband transmit-receive antennas and dual-band RF pulses. *NMR Biomed.* **2015**, *28*, 1433–1442. [CrossRef] [PubMed]
18. Zhang, Y.N.; Fowler, K.J.; Hamilton, G.; Cui, J.Y.; Sy, E.Z.; Balanay, M.; Hooker, J.C.; Szeverenyi, N.; Sirlin, C.B. Liver fat imaging–A clinical overview of ultrasound, CT, and MR imaging. *Br. J. Radiol.* **2018**, *91*, 20170959. [CrossRef]
19. Szczepaniak, L.S.; Nurenberg, P.; Leonard, D.; Browning, J.D.; Reingold, J.S.; Grundy, S.; Hobbs, H.H.; Dobbins, R.L. Magnetic resonance spectroscopy to measure hepatic triglyceride content: Prevalence of hepatic steatosis in the general population. *Am. J. Physiol. Metab.* **2005**, *288*, E462–E468. [CrossRef]
20. Di Martino, M.; Pacifico, L.; Bezzi, M.; Di Miscio, R.; Sacconi, B.; Chiesa, C.; Catalano, C. Comparison of magnetic resonance spectroscopy, proton density fat fraction and histological analysis in the quantification of liver steatosis in children and adolescents. *World J. Gastroenterol.* **2016**, *22*, 8812–8819. [CrossRef]
21. Caussy, C.; Reeder, S.B.; Sirlin, C.B.; Loomba, R. Noninvasive, Quantitative Assessment of Liver Fat by MRI-PDFF as an Endpoint in NASH Trials. *Hepatology* **2018**, *68*, 763–772. [CrossRef]
22. Caussy, C.; Alquiraish, M.H.; Nguyen, P.; Hernandez, C.; Cepin, S.; Fortney, L.E.; Ajmera, V.; Bettencourt, R.; Collier, S.; Hooker, J.; et al. Optimal threshold of controlled attenuation parameter with MRI-PDFF as the gold standard for the detection of hepatic steatosis. *Hepatology* **2017**, *67*, 1348–1359. [CrossRef] [PubMed]
23. Roumans, K.H.M.; Lindeboom, L.; Veeraiah, P.; Remie, C.M.E.; Phielix, E.; Havekes, B.; Bruls, Y.; Brouwers, M.C.G.J.; Ståhlman, M.; Alssema, M.; et al. Hepatic saturated fatty acid fraction is associated with de novo lipogenesis and hepatic insulin resistance. *Nat. Commun.* **2020**, *11*, 1891. [CrossRef] [PubMed]
24. Gajdosik, M.; Chadzynski, G.L.; Hangel, G.; Mlynarik, V.; Chmelík, M.; Valkovič, L.; Bogner, W.; Pohmann, R.; Scheffler, K.; Trattnig, S.; et al. Ultrashort-TE stimulated echo acquisition mode (STEAM) improves the quantification of lipids and fatty acid chain unsaturation in the human liver at 7 T. *NMR Biomed.* **2015**, *28*, 1283–1293. [CrossRef]
25. Weis, J.; Kullberg, J.; Ahlström, H. Multiple breath-hold proton spectroscopy of human liver at 3T: Relaxation times and concentrations of glycogen, choline, and lipids. *J. Magn. Reson. Imaging* **2017**, *47*, 410–417. [CrossRef] [PubMed]
26. Ouwerkerk, R.; Pettigrew, R.I.; Gharib, A. Liver Metabolite Concentrations Measured with1H MR Spectroscopy. *Radiology* **2012**, *265*, 565–575. [CrossRef] [PubMed]
27. Ter Voert, E.; Heijmen, L.; van Asten, J.J.A.; Wright, A.J.; Nagtegaal, I.D.; Punt, C.J.A.; de Wilt, J.H.W.; van Laarhoven, H.W.M.; Heerschap, A. Levels of choline-containing compounds in normal liver and liver metastases of colorectal cancer as recorded by H-1 MRS. *NMR Biomed.* **2019**, *32*, e4035. [CrossRef]
28. Chen, W.; Avison, M.J.; Zhu, X.H.; Shulman, R.G. NMR studies of proton NOEs in glycogen. *Biochemistry* **1993**, *32*, 11483–11487. [CrossRef]
29. Zhou, Y.; van Zijl, P.C.M.; Xu, X.; Xu, J.; Li, Y.; Chen, L.; Yadav, N.N. Magnetic resonance imaging of glycogen using its magnetic coupling with water. *Proc. Natl. Acad. Sci. USA* **2020**, *117*, 3144–3149. [CrossRef] [PubMed]
30. Bowers, J.L.; Lanir, A.; Metz, K.R.; Kruskal, J.B.; Lee, R.G.; Balschi, J.; Federman, M.; Khettry, U.; Clouse, M.E. 23Na- and ^{31}P-NMR studies of perfused mouse liver during nitrogen hypoxia. *Am. J. Physiol. Liver Physiol.* **1992**, *262*, G636–G644. [CrossRef]
31. Kitai, T.; Tanaka, A.; Terasaki, M.; Okamoto, R.; Ozawa, K.; Morikawa, S.; Inubushi, T. Energy metabolism of the liver in brain dead dogs assessed by ^{31}P-NMR spectroscopy and arterial ketone body ratio. *Life Sci.* **1991**, *49*, 511–518. [CrossRef]
32. Buchli, R.; Meier, D.; Martin, E.; Boesiger, P. Assessment of absolute metabolite concentrations in human tissue by P-31 MRS in vivo. Part II: Muscle, liver, kidney. *Magn. Reson. Med.* **1994**, *32*, 453–458. [CrossRef] [PubMed]
33. Traussnigg, S.; Kienbacher, C.; Gajdosik, M.; Valkovič, L.; Halilbasic, E.; Stift, J.; Rechling, C.; Hofer, H.; Steindl-Munda, P.; Ferenci, P.; et al. Ultra-high-field magnetic resonance spectroscopy in non-alcoholic fatty liver disease: Novel mechanistic and diagnostic insights of energy metabolism in non-alcoholic steatohepatitis and advanced fibrosis. *Liver Int.* **2017**, *37*, 1544–1553. [CrossRef]
34. Buehler, T.; Kreis, R.; Boesch, C. Comparison of ^{31}P saturation and inversion magnetization transfer in human liver and skeletal muscle using a clinical MR system and surface coils. *NMR Biomed.* **2014**, *28*, 188–199. [CrossRef] [PubMed]
35. Campbell, S.; Jones, K.A.; Shulman, R.G. In vivo ^{31}P nuclear magnetic resonance saturation transfer measurements of phosphate exchange reactions in the yeast Saccharomyces cerevisiae. *FEBS Lett.* **1985**, *193*, 189–193. [CrossRef]
36. Alger, J.R.; Hollander, J.A.D.; Shulman, R.G. In vivo phosphorus-31 nuclear magnetic resonance saturation transfer studies of adenosinetriphosphatase kinetics in Saccharomyces cerevisiae. *Biochemistry* **1982**, *21*, 2957–2963. [CrossRef]
37. Laufs, A.; Livingstone, R.; Nowotny, B.; Nowotny, P.; Wickrath, F.; Giani, G.; Bunke, J.; Roden, M.; Hwang, J.-H. Quantitative liver 31 P magnetic resonance spectroscopy at 3T on a clinical scanner. *Magn. Reson. Med.* **2013**, *71*, 1670–1675. [CrossRef] [PubMed]
38. Ruiz-Cabello, J.; Cohen, J.S. Phospholipid metabolites as indicators of cancer cell function. *NMR Biomed.* **1992**, *5*, 226–233. [CrossRef] [PubMed]
39. Daly, P.F.; Lyon, R.C.; Faustino, P.J.; Cohen, J.S. Phospholipid metabolism in cancer cells monitored by ^{31}P NMR spectroscopy. *J. Biol. Chem.* **1987**, *262*, 14875–14878. [CrossRef]

40. Yuan, Z.; Ye, X.-D.; Dong, S.; Xu, L.-C.; Xiao, X.-S. Evaluation of Early Imaging Response After Chemoembolization of Hepatocellular Carcinoma by Phosphorus-31 Magnetic Resonance Spectroscopy—Initial Experience. *J. Vasc. Interv. Radiol.* **2011**, *22*, 1166–1173. [CrossRef] [PubMed]
41. Taylor-Robinson, S.D.; Sargentoni, J.; Bell, J.D.; Saeed, N.; Changani, K.K.; Davidson, B.R.; Rolles, K.; Burroughs, A.K.; Hodgson, H.J.F.; Foster, C.S.; et al. In vivo and in vitro hepatic ^{31}P magnetic resonance spectroscopy and electron microscopy of the cirrhotic liver. *Liver Int.* **2008**, *17*, 198–209. [CrossRef] [PubMed]
42. Cox, I.; Menon, D.K.; Sargentoni, J.; Bryant, D.J.; Collins, A.G.; Coutts, G.A.; Iles, R.A.; Bell, J.D.; Benjamin, I.; Gilbey, S.; et al. Phosphorus-31 magnetic resonance spectroscopy of the human liver using chemical shift imaging techniques. *J. Hepatol.* **1992**, *14*, 265–275. [CrossRef]
43. Bernardo-Seisdedos, G.; Bilbao, J.; Fernández-Ramos, D.; Lopitz-Otsoa, F.; de Juan, V.G.; Bizkarguenaga, M.; Mateos, B.; Fondevila, M.F.; Abril-Fornaguera, J.; Diercks, T.; et al. Metabolic Landscape of the Mouse Liver by Quantitative 31 P Nuclear Magnetic Resonance Analysis of the Phosphorome. *Hepatology* **2020**, *74*, 148–163. [CrossRef] [PubMed]
44. Chmelik, M.; Povazan, M.; Kršśák, M.; Gruber, S.; Tkačov, M.; Trattnig, S.; Bogner, W. In vivo ^{31}P magnetic resonance spectroscopy of the human liver at 7 T: An initial experience. *NMR Biomed.* **2014**, *27*, 478–485. [CrossRef] [PubMed]
45. Purvis, L.A.; Clarke, W.; Valkovič, L.; Levick, C.; Pavlides, M.; Barnes, E.; Cobbold, J.F.; Robson, M.D.; Rodgers, C.T. Phosphodiester content measured in human liver by in vivo 31 P MR spectroscopy at 7 tesla. *Magn. Reson. Med.* **2017**, *78*, 2095–2105. [CrossRef] [PubMed]
46. Valkovič, L.; Chmelík, M.; Kršśák, M. In-vivo 31 P-MRS of skeletal muscle and liver: A way for non-invasive assessment of their metabolism. *Anal. Biochem.* **2017**, *529*, 193–215. [CrossRef]
47. Bierwagen, A.; Begovatz, P.; Nowotny, P.; Markgraf, D.; Nowotny, B.; Koliaki, C.; Giani, G.; Klüppelholz, B.; Lundbom, J.; Roden, M. Characterization of the peak at 2.06 ppm in ^{31}P magnetic resonance spectroscopy of human liver: Phosphoenolpyruvate or phosphatidylcholine? *NMR Biomed.* **2015**, *28*, 898–905. [CrossRef] [PubMed]
48. Chmelík, M.; Valkovic, L.; Wolf, P.; Bogner, W.; Gajdosik, M.; Halilbasic, E.; Gruber, S.; Trauner, M.; Krebs, M.; Trattnig, S.; et al. Phosphatidylcholine contributes to in vivo ^{31}P MRS signal from the human liver. *Eur. Radiol.* **2015**, *25*, 2059–2066. [CrossRef]
49. Kupriyanova, Y.; Zaharia, O.P.; Bobrov, P.; Karusheva, Y.; Burkart, V.; Szendroedi, J.; Hwang, J.-H.; Roden, M.; Al-Hasani, H.; Buyken, A.; et al. Early changes in hepatic energy metabolism and lipid content in recent-onset type 1 and 2 diabetes mellitus. *J. Hepatol.* **2020**, *74*, 1028–1037. [CrossRef]
50. Ms, L.P.; Gajdosik, M.; Wolf, P.; Smajis, S.; Fellinger, P.; Kuehne, A.; Krumpolec, P.; Trattnig, S.; Winhofer, Y.; Krebs, M.; et al. Absolute Quantification of Phosphor-Containing Metabolites in the Liver Using ^{31}P MRSI and Hepatic Lipid Volume Correction at 7T Suggests No Dependence on Body Mass Index or Age. *J. Magn. Reson. Imaging* **2018**, *49*, 597–607. [CrossRef]
51. Hakkarainen, A.; Lundbom, J.; Tuominen, E.K.; Taskinen, M.-R.; Pietiläinen, K.H.; Lundbom, N. Measuring short-term liver metabolism non-invasively: Postprandial and post-exercise 1H and ^{31}P MR spectroscopy. *Magma Magn. Reson. Mater. Phys. Biol. Med.* **2014**, *28*, 57–66. [CrossRef] [PubMed]
52. Bawden, S.; Stephenson, M.; Ciampi, E.; Hunter, K.; Marciani, L.; Macdonald, I.; Aithal, G.; Morris, P.; Gowland, P. Investigating the effects of an oral fructose challenge on hepatic ATP reserves in healthy volunteers: A ^{31}P MRS study. *Clin. Nutr.* **2015**, *35*, 645–649. [CrossRef] [PubMed]
53. Boesch, C.; Elsing, C.; Wegmüller, H.; Felblinger, J.; Vock, P.; Reichen, J. Effect of ethanol and fructose on liver metabolism: A dynamic (31) phosphorus magnetic resonance spectroscopy study in normal volunteers. *Magn. Reson. Imaging* **1997**, *15*, 1067–1077. [CrossRef]
54. Sevastianova, K.; Hakkarainen, A.; Kotronen, A.; Cornér, A.; Arkkila, P.; Arola, J.; Westerbacka, J.; Bergholm, R.; Lundbom, J.; Lundbom, N.; et al. Nonalcoholic Fatty Liver Disease: Detection of Elevated Nicotinamide Adenine Dinucleotide Phosphate with in Vivo 3.0-T31P MR Spectroscopy with Proton Decoupling. *Radiology* **2010**, *256*, 466–473. [CrossRef] [PubMed]
55. Changani, K.K. Evidence for altered hepatic gluconeogenesis in patients with cirrhosis using in vivo 31-phosphorus magnetic resonance spectroscopy. *Gut* **2001**, *49*, 557–564. [CrossRef]
56. Chu, W.C.W.; Lam, W.W.M.; Lee, K.-H.; Yeung, D.K.W.; Sihoe, J.; Yeung, C.-K. Phosphorus-31 MR Spectroscopy in Pediatric Liver Transplant Recipients: A Noninvasive Assessment of Graft Status with Correlation with Liver Function Tests and Liver Biopsy. *Am. J. Roentgenol.* **2005**, *184*, 1624–1629. [CrossRef] [PubMed]
57. Leij-Halfwerk, S.; Agteresch, H.J.; Sijens, P.E.; Dagnelie, P.C. Adenosine triphosphate infusion increases liver energy status in advanced lung cancer patients: Anin vivo31P magnetic resonance spectroscopy study. *Hepatology* **2002**, *35*, 421–424. [CrossRef]
58. Petersen, K.F.; West, A.B.; Reuben, A.; Rothman, D.L.; Shulman, G.I. Noninvasive assessment of hepatic triglyceride content in humans with 13C nuclear magnetic resonance spectroscopy. *Hepatology* **1996**, *24*, 114–117. [CrossRef]
59. Stender, S.; Zaha, V.; Malloy, C.R.; Sudderth, J.; DeBerardinis, R.J.; Park, J.M. Assessment of Rapid Hepatic Glycogen Synthesis in Humans Using Dynamic 13 C Magnetic Resonance Spectroscopy. *Hepatol. Commun.* **2020**, *4*, 425–433. [CrossRef]
60. Skamarauskas, J.T.; Oakley, F.; Smith, F.E.; Bawn, C.; Dunn, M.; Vidler, D.S.; Clemence, M.; Blain, P.G.; Taylor, R.; Gamcsik, M.P.; et al. Noninvasivein vivomagnetic resonance measures of glutathione synthesis in human and rat liver as an oxidative stress biomarker. *Hepatology* **2013**, *59*, 2321–2330. [CrossRef]
61. Petersen, K.F.; Cline, G.W.; Gerard, D.P.; Magnusson, I.; Rothman, D.L.; Shulman, G. Contribution of net hepatic glycogen synthesis to disposal of an oral glucose load in humans. *Metabolism* **2001**, *50*, 598–601. [CrossRef]

62. Befroy, D.E.; Perry, R.J.; Jain, N.; Dufour, S.; Cline, G.W.; Trimmer, J.K.; Brosnan, J.; Rothman, D.L.; Petersen, K.F.; Shulman, G.I. Direct assessment of hepatic mitochondrial oxidative and anaplerotic fluxes in humans using dynamic 13C magnetic resonance spectroscopy. *Nat. Med.* **2013**, *20*, 98–102. [CrossRef] [PubMed]
63. Lindeboom, L.; De Graaf, R.A.; Nabuurs, C.I.; Van Ewijk, P.A.; Hesselink, M.K.; Wildberger, J.E.; Schrauwen, P.; Schrauwen-Hinderling, V.B. Quantum coherence spectroscopy to measure dietary fat retention in the liver. *JCI Insight* **2016**, *1*, e84671. [CrossRef]
64. De Graaf, R.A. Theoretical and experimental evaluation of broadband decoupling techniques for in vivo nuclear magnetic resonance spectroscopy. *Magn. Reson. Med.* **2005**, *53*, 1297–1306. [CrossRef] [PubMed]
65. Kacerovsky, M.; Jones, J.; Schmid, A.I.; Barosa, C.; Lettner, A.; Kacerovsky-Bielesz, G.; Szendroedi, J.; Chmelik, M.; Nowotny, P.; Chandramouli, V.; et al. Postprandial and Fasting Hepatic Glucose Fluxes in Long-Standing Type 1 Diabetes. *Diabetes* **2011**, *60*, 1752–1758. [CrossRef] [PubMed]
66. Matyka, K.; Dixon, R.M.; Mohn, A.; Rajagopalan, B.; Shmueli, E.; Styles, P.; Dunger, D.B. Daytime liver glycogen accumulation, measured by C-13 magnetic resonance spectroscopy, in young children with Type 1 diabetes mellitus. *Diabet. Med.* **2001**, *18*, 659–662. [CrossRef]
67. Krssak, M.; Brehm, A.; Bernroider, E.; Anderwald, C.H.; Nowotny, P.; Man, C.D.; Cobelli, C.; Cline, G.W.; Shulman, G.; Waldhäusl, W.; et al. Alterations in Postprandial Hepatic Glycogen Metabolism in Type 2 Diabetes. *Diabetes* **2004**, *53*, 3048–3056. [CrossRef] [PubMed]
68. Sarabhai, T.; Kahl, S.; Szendroedi, J.; Markgraf, D.F.; Zaharia, O.-P.; Barosa, C.; Herder, C.; Wickrath, F.; Bobrov, P.; Hwang, J.-H.; et al. Monounsaturated fat rapidly induces hepatic gluconeogenesis and whole-body insulin resistance. *JCI Insight* **2020**, *5*, 4520. [CrossRef] [PubMed]
69. Krššák, M. 13C MRS in Human Tissue. *eMagRes* **2016**, *17*, 1027–1038. [CrossRef]
70. Bischof, M.G.; Bernroider, E.; Krssak, M.; Krebs, M.; Stingl, H.; Nowotny, P.; Yu, C.; Shulman, G.; Waldhäusl, W.; Roden, M. Hepatic Glycogen Metabolism in Type 1 Diabetes After Long-Term Near Normoglycemia. *Diabetes* **2002**, *51*, 49–54. [CrossRef]
71. Bischof, M.G.; Krssak, M.; Krebs, M.; Bernroider, E.; Stingl, H.; Waldhäusl, W.; Roden, M. Effects of Short-Term Improvement of Insulin Treatment and Glycemia on Hepatic Glycogen Metabolism in Type 1 Diabetes. *Diabetes* **2001**, *50*, 392–398. [CrossRef]
72. Hernández, E.; Kahl, S.; Seelig, A.; Begovatz, P.; Irmler, M.; Kupriyanova, Y.; Nowotny, B.; Nowotny, P.; Herder, C.; Barosa, C.; et al. Acute dietary fat intake initiates alterations in energy metabolism and insulin resistance. *J. Clin. Investig.* **2017**, *127*, 695–708. [CrossRef] [PubMed]
73. Janssens, S.; Jonkers, R.A.M.; Groen, A.K.; Nicolay, K.; van Loon, L.J.; Prompers, J.J. Effects of acute exercise on lipid content and dietary lipid uptake in liver and skeletal muscle of lean and diabetic rats. *Am. J. Physiol. Metab.* **2015**, *309*, E874–E883. [CrossRef] [PubMed]
74. Veeraiah, P.; Brouwers, K.; Wildberger, J.E.; Schrauwen-Hinderling, V.B.; Lindeboom, L. Application of a BIlinear Rotation Decoupling (BIRD) filter in combination with J-difference editing for indirect 13 C measurements in the human liver. *Magn. Reson. Med.* **2020**, *84*, 2911–2917. [CrossRef]
75. Keshari, K.; Wilson, D.M. Chemistry and biochemistry of13C hyperpolarized magnetic resonance using dynamic nuclear polarization. *Chem. Soc. Rev.* **2013**, *43*, 1627–1659. [CrossRef] [PubMed]
76. Stewart, N.J.; Nakano, H.; Sugai, S.; Tomohiro, M.; Kase, Y.; Uchio, Y.; Yamaguchi, T.; Matsuo, Y.; Naganuma, T.; Takeda, N.; et al. Hyperpolarized 13 C Magnetic Resonance Imaging of Fumarate Metabolism by Parahydrogen-induced Polarization: A Proof-of-Concept in vivo Study. *ChemPhysChem* **2021**, *22*, 915–923. [CrossRef] [PubMed]
77. Wang, Z.J.; Ohliger, M.A.; Larson, P.E.Z.; Gordon, J.W.; Bok, R.A.; Slater, J.; Villanueva-Meyer, J.E.; Hess, C.P.; Kurhanewicz, J.; Vigneron, D.B. Hyperpolarized 13C MRI: State of the Art and Future Directions. *Radiology* **2019**, *291*, 273–284. [CrossRef]
78. Kurhanewicz, J.; Vigneron, D.B.; Ardenkjaer-Larsen, J.H.; Bankson, J.A.; Brindle, K.; Cunningham, C.; Gallagher, F.A.; Keshari, K.R.; Kjaer, A.; Laustsen, C.; et al. Hyperpolarized 13C MRI: Path to Clinical Translation in Oncology. *Neoplasia* **2018**, *21*, 1–16. [CrossRef] [PubMed]
79. De Feyter, H.M.; Thomas, M.A.; Behar, K.L.; de Graaf, R.A. NMR visibility of deuterium-labeled liver glycogen in vivo. *Magn. Reson. Med.* **2021**, *86*, 62–68. [CrossRef]
80. De Feyter, H.M.; Behar, K.L.; Corbin, Z.A.; Fulbright, R.K.; Brown, P.B.; McIntyre, S.; Nixon, T.W.; Rothman, D.L.; de Graaf, R.A. Deuterium metabolic imaging (DMI) for MRI-based 3D mapping of metabolism in vivo. *Sci. Adv.* **2018**, *4*, eaat7314. [CrossRef]
81. De Graaf, R.A.; Thomas, M.A.; Behar, K.L.; De Feyter, H.M. Characterization of Kinetic Isotope Effects and Label Loss in Deuterium-Based Isotopic Labeling Studies. *ACS Chem. Neurosci.* **2020**, *12*, 234–243. [CrossRef]
82. Rose, I.A.; Oconnell, E.L. Intramolecular Hydrogen Transfer in Phosphoglucose Isomerase Reaction. *J. Biol. Chem.* **1961**, *236*, 3086. [CrossRef]
83. Wolf, W.; Albright, M.J.; Silver, M.S.; Weber, H.; Reichardt, U.; Sauer, R. Fluorine-19 NMR spectroscopic studies of the metabolism of 5-fluorouracil in the liver of patients undergoing chemotherapy. *Magn. Reson. Imaging* **1987**, *5*, 165–169. [CrossRef]
84. Peters, G.J.; Lankelma, J.; Kok, R.M.; Noordhuis, P.; Van Groeningen, C.J.; Van Der Wilt, C.L.; Meyer, S.; Pinedo, H.M. Prolonged retention of high concentrations of 5-fluorouracil in human and murine tumors as compared with plasma. *Cancer Chemother. Pharmacol.* **1993**, *31*, 269–276. [CrossRef]
85. Li, C.-W.; Gonen, O. Simultaneous 3D NMR spectroscopy of fluorine and phosphorus in human liver during 5-fluorouracil chemotherapy. *Magn. Reson. Med.* **1996**, *35*, 841–847. [CrossRef] [PubMed]

86. Murphy-Boesch, J.; He, C.-W.L.L.; Padavic-Shaller, K.A.; Negendank, W.; Brown, T.R. Proton-decoupled ^{19}F spectroscopy of 5-FU catabolites in human liver. *Magn. Reson. Med.* **1997**, *37*, 321–326. [CrossRef] [PubMed]
87. Wolf, W.; Waluch, V.; Presant, C.A. Non-invasive ^{19}F-NMRS of 5-fluorouracil in pharmacokinetics and pharmacodynamic studies. *NMR Biomed.* **1998**, *11*, 380–387. [CrossRef]
88. Mohankrishnan, P.; Hutchins, L.; Nauke, S.; Sprigg, J.; Cardwell, D.; Williamson, M.R.; Komoroski, R.A.; Jagannathan, N.R. Metabolism of 5-fluorouracil in human liver: An in vivo F-19 NMR study. *Curr. Sci.* **1999**, *76*, 677–680.
89. Schlemmer, H.-P.; Bachert, P.; Semmler, W.; Hohenberger, P.; Schlag, P.; Lorenz, W.J.; van Kaick, G. Drug monitoring of 5-fluorouracil: In vivo ^{19}F NMR study during 5-FU chemotherapy in patients with metastases of colorectal adenocarcinoma. *Magn. Reson. Imaging* **1994**, *12*, 497–511. [CrossRef]
90. Findlay, M.P.N.; Leach, M.O.; Cunningham, D.; Collins, D.; Payne, G.S.; Glaholm, J.; Mansi, J.L.; McCready, V.R. The non-invasive monitoring of low dose, infusional 5-fluorouracil and its modulation by interferon-α using in vivo ^{19}F magnetic resonance spectroscopy in patients with colorectal cancer: A pilot study. *Ann. Oncol.* **1993**, *4*, 597–602. [CrossRef]
91. Harada, M.; Nishitani, H.; Koga, K.; Miura, I.; Kimura, A. Comparative Studies on the Metabolism of New Fluorinated Pyrimidine Drugs in the Liver by in vivo ^{19}F Magnetic Resonance Spectroscopic Observation. *Jpn. J. Cancer Res.* **1993**, *84*, 197–202. [CrossRef]
92. Klomp, D.; Van Laarhoven, H.; Scheenen, T.; Kamm, Y.; Heerschap, A. Quantitative ^{19}F MR spectroscopy at 3 T to detect heterogeneous capecitabine metabolism in human liver. *NMR Biomed.* **2006**, *20*, 485–492. [CrossRef] [PubMed]
93. Payne, G.S.; Collins, D.J.; Loynds, P.; Mould, G.; Murphy, P.S.; Dzik-Jurasz, A.S.K.; Kessar, P.; Haque, N.; Yamaguchi, M.; Atarashi, S.; et al. Quantitative assessment of the hepatic pharmacokinetics of the antimicrobial sitafloxacin in humans using in vivo ^{19}F magnetic resonance spectroscopy. *Br. J. Clin. Pharmacol.* **2005**, *59*, 244–248. [CrossRef]
94. Bilecen, D.; Schulte, A.-C.; Kaspar, A.; Küstermann, E.; Seelig, J.; von Elverfeldt, D.; Scheffler, K. Detection of the non-steroidal anti-inflammatory drug niflumic acid in humans: A combined ^{19}F-MRSin vivoandin vitrostudy. *NMR Biomed.* **2003**, *16*, 144–151. [CrossRef] [PubMed]
95. Marco-Rius, I.; Wright, A.J.; Hu, D.-E.; Savic, D.; Miller, J.J.; Timm, K.N.; Tyler, D.; Brindle, K.M.; Comment, A. Probing hepatic metabolism of [2-13C]dihydroxyacetone in vivo with 1H-decoupled hyperpolarized 13C-MR. *Magma Magn. Reson. Mater. Physics Biol. Med.* **2020**, *34*, 49–56. [CrossRef] [PubMed]
96. Moreno, K.X.; Satapati, S.; DeBerardinis, R.J.; Burgess, S.C.; Malloy, C.; Merritt, M.E. Real-time Detection of Hepatic Gluconeogenic and Glycogenolytic States Using Hyperpolarized [2-13C]Dihydroxyacetone. *J. Biol. Chem.* **2014**, *289*, 35859–35867. [CrossRef]
97. Ragavan, M.; McLeod, M.; Giacalone, A.; Merritt, M. Hyperpolarized Dihydroxyacetone Is a Sensitive Probe of Hepatic Gluconeogenic State. *Metabolites* **2021**, *11*, 441. [CrossRef]
98. Merritt, M.E.; Harrison, C.; Sherry, D.; Malloy, C.; Burgess, S.C. Flux through hepatic pyruvate carboxylase and phosphoenolpyruvate carboxykinase detected by hyperpolarized 13C magnetic resonance. *Proc. Natl. Acad. Sci. USA* **2011**, *108*, 19084–19089. [CrossRef]
99. Chen, J.; Hackett, E.P.; Kovacs, Z.; Malloy, C.R.; Park, J.M. Assessment of hepatic pyruvate carboxylase activity using hyperpolarized [1-13 C]-l-lactate. *Magn. Reson. Med.* **2020**, *85*, 1175–1182. [CrossRef]
100. Høyer, K.F.; Laustsen, C.; Ringgaard, S.; Qi, H.; Mariager, C.; Nielsen, T.S.; Sundekilde, U.; Treebak, J.T.; Jessen, N.; Stødkilde-Jørgensen, H. Assessment of mouse liver [1-13C]pyruvate metabolism by dynamic hyperpolarized MRS. *J. Endocrinol.* **2019**, *242*, 251–260. [CrossRef]
101. Moreno, K.X.; Harrison, C.E.; Merritt, M.E.; Kovacs, Z.; Malloy, C.R.; Sherry, A.D. Hyperpolarized delta- 1-C-13 gluconolac-tone as a probe of the pentose phosphate pathway. *NMR Biomed.* **2017**, *30*, e3713. [CrossRef]
102. Wibowo, A.; Park, J.M.; Liu, S.-C.; Khosla, C.; Spielman, D.M. Real-Time in Vivo Detection of H_2O_2 Using Hyperpolarized 13C-Thiourea. *ACS Chem. Biol.* **2017**, *12*, 1737–1742. [CrossRef] [PubMed]
103. Park, J.M.; Khemtong, C.; Liu, S.; Hurd, R.E.; Spielman, D.M. In vivo assessment of intracellular redox state in rat liver using hyperpolarized [1-13 C]Alanine. *Magn. Reson. Med.* **2017**, *77*, 1741–1748. [CrossRef] [PubMed]
104. Rardin, M.J.; He, W.; Nishida, Y.; Newman, J.C.; Carrico, C.; Danielson, S.R.; Guo, A.; Gut, P.; Sahu, A.K.; Li, B.; et al. SIRT5 Regulates the Mitochondrial Lysine Succinylome and Metabolic Networks. *Cell Metab.* **2013**, *18*, 920–933. [CrossRef] [PubMed]
105. Indiveri, C.; Iacobazzi, V.; Tonazzi, A.; Giangregorio, N.; Infantino, V.; Convertini, P.; Console, L.; Palmieri, F. The mitochondrial carnitine/acylcarnitine carrier: Function, structure and physiopathology. *Mol. Asp. Med.* **2011**, *32*, 223–233. [CrossRef]
106. Wanders, R.J.A.; Vreken, P.; Boer, M.E.J.D.; Wijburg, F.A.; Van Gennip, A.H.; Ijlst, L. Disorders of mitochondrial fatty acyl-CoA β-oxidation. *J. Inherit. Metab. Dis.* **1999**, *22*, 442–487. [CrossRef] [PubMed]
107. Von Morze, C.; Engelbach, J.A.; Reed, G.D.; Chen, A.P.; Quirk, J.D.; Blazey, T.; Mahar, R.; Malloy, C.R.; Garbow, J.R.; Merritt, M.E. 15 N-carnitine, a novel endogenous hyperpolarized MRI probe with long signal lifetime. *Magn. Reson. Med.* **2020**, *85*, 1814–1820. [CrossRef] [PubMed]
108. Von Morze, C.; Allu, P.K.R.; Chang, G.Y.; Marco-Rius, I.; Milshteyn, E.; Wang, Z.J.; Ohliger, M.A.; Gleason, C.E.; Kurhanewicz, J.; Vigneron, D.B.; et al. Non-invasive detection of divergent metabolic signals in insulin deficiency vs. insulin resistance in vivo. *Sci. Rep.* **2018**, *8*, 1–12. [CrossRef]
109. Erratum: Global cancer statistics 2018: GLOBOCAN estimates of incidence and mortality worldwide for 36 cancers in 185 countries. *CA Cancer J. Clin.* **2020**, *70*, 313. [CrossRef] [PubMed]
110. Paik, J.M.; Golabi, P.; Younossi, Y.; Mishra, A.; Younossi, Z.M. Changes in the Global Burden of Chronic Liver Diseases From 2012 to 2017: The Growing Impact of NAFLD. *Hepatology* **2020**, *72*, 1605–1616. [CrossRef] [PubMed]

111. Jensen, P.R.; Serra, S.C.; Miragoli, L.; Karlsson, M.; Cabella, C.; Poggi, L.; Venturi, L.; Tedoldi, F.; Lerche, M.H. Hyperpolarized [1,3-13C2]ethyl acetoacetate is a novel diagnostic metabolic marker of liver cancer. *Int. J. Cancer* **2014**, *136*, E117–E126. [CrossRef] [PubMed]
112. Maptue, N.; Jiang, W.; Harrison, C.; Funk, A.M.; Sharma, G.; Malloy, C.R.; Sherry, D.; Khemtong, C. Esterase-Catalyzed Production of Hyperpolarized 13C-Enriched Carbon Dioxide in Tissues for Measuring pH. *ACS Sens.* **2018**, *3*, 2232–2236. [CrossRef] [PubMed]
113. Perkons, N.R.; Kiefer, R.M.; Noji, M.C.; Pourfathi, M.; Ackerman, D.; Siddiqui, S.; Tischfield, D.; Profka, E.; Johnson, O.; Pickup, S.; et al. Hyperpolarized Metabolic Imaging Detects Latent Hepatocellular Carcinoma Domains Surviving Locoregional Therapy. *Hepatology* **2019**, *72*, 140–154. [CrossRef] [PubMed]